Crystal Structure of the Measles Virus Nucleoprotein Core in Complex with an N-terminal Region of Phosphoprotein

Guryanov, Sergey

2016

Guryanov , S , Liljeroos , L J P , Kasaragod , P , Kajander , T A & Butcher , S J 2016 , ' Crystal Structure of the Measles Virus Nucleoprotein Core in Complex with an N-terminal Region of Phosphoprotein ' , Journal of Virology , vol. 90 , no. 6 , pp. 2849-2857 . https://doi.org/10.1128/JVI.02865-1

http://hdl.handle.net/10138/223843
https://doi.org/10.1128/JVI.02865-15

publishedVersion

AMERICAN SOCIETY FOR MICROBIOLOGY | Journal of Virology

Crystal Structure of the Measles Virus Nucleoprotein Core in Complex with an N-Terminal Region of Phosphoprotein

Sergey G. Guryanov,[b] Lassi Liljeroos,[a,b]* Prasad Kasaragod,[b] Tommi Kajander,[b] Sarah J. Butcher[a,b]

Department of Biological Sciences[a] and Institute of Biotechnology,[b] University of Helsinki, Helsinki, Finland

ABSTRACT

The enveloped negative-stranded RNA virus measles virus (MeV) is an important human pathogen. The nucleoprotein (N^0) assembles with the viral RNA into helical ribonucleocapsids (NC) which are, in turn, coated by a helical layer of the matrix protein. The viral polymerase complex uses the NC as its template. The N^0 assembly onto the NC and the activity of the polymerase are regulated by the viral phosphoprotein (P). In this study, we pulled down an N^0_{1-408} fragment lacking most of its C-terminal tail domain by several affinity-tagged, N-terminal P fragments to map the N^0-binding region of P to the first 48 amino acids. We showed biochemically and using P mutants the importance of the hydrophobic interactions for the binding. We fused an N^0 binding peptide, P_{1-48}, to the C terminus of an N^0_{21-408} fragment lacking both the N-terminal peptide and the C-terminal tail of N protein to reconstitute and crystallize the N^0-P complex. We solved the X-ray structure of the resulting N^0-P chimeric protein at a resolution of 2.7 Å. The structure reveals the molecular details of the conserved N^0-P interface and explains how P chaperones N^0, preventing both self-assembly of N^0 and its binding to RNA. Finally, we propose a model for a preinitiation complex for RNA polymerization.

IMPORTANCE

Measles virus is an important, highly contagious human pathogen. The nucleoprotein N binds only to viral genomic RNA and forms the helical ribonucleocapsid that serves as a template for viral replication. We address how N is regulated by another protein, the phosphoprotein (P), to prevent newly synthesized N from binding to cellular RNA. We describe the atomic model of an N-P complex and compare it to helical ribonucleocapsid. We thus provide insight into how P chaperones N and helps to start viral RNA synthesis. Our results provide a new insight into mechanisms of paramyxovirus replication. New data on the mechanisms of phosphoprotein chaperone action allows better understanding of virus genome replication and nucleocapsid assembly. We describe a conserved structural interface for the N-P interaction which could be a target for drug development to treat not only measles but also potentially other paramyxovirus diseases.

Measles virus (MeV) belongs to the *Paramyxoviridae* family, which includes several other human pathogens, like respiratory syncytial (RSV), mumps, and parainfluenza viruses. It has a helical ribonucleocapsid (NC) containing a nonsegmented single-strand RNA (ssRNA) genome wrapped around the outside the nucleoprotein (N) helix (1). The helical NC is active in both transcription and replication. During virus assembly, the matrix protein forms an additional helix covering the majority of the NC, potentially inhibiting transcription and promoting packaging into progeny virions (2). There are still only limited data on the detailed molecular interactions required to go from replication initiation to packaging of nascent RNA. The availability of N in a chaperoned, assembly-competent state with the phosphoprotein (P) versus the assembled helical state is thought to be critical to these processes.

N is composed of an ordered N_{CORE} region (amino acids 1 to 391) and an intrinsically disordered N_{TAIL} region (amino acids 392 to 525) (Fig. 1A). N_{CORE} contains two domains (N_{NTD} and N_{CTD}) flanked by N- and C-terminal arms (NT_{arm} and CT_{arm}). A recent atomic model of the MeV NC from a cryo-electron microscopic (cryo-EM) reconstruction revealed the molecular details of N oligomerization mediated by exchange of the NT_{arm} and CT_{arm} between consecutive N monomers and showed the RNA-binding site on the groove between the two N_{CORE} domains (1).

P is a modular protein comprised of an ordered tetramerization domain, MD (amino acids 304 to 377), forming a parallel four-helix coiled-coil (3), and an extreme C-terminal domain (CTD), XD, alternating with disordered regions (Fig. 1A). For transcription and replication, the RNA polymerase (L) in complex with P attaches to the NC via an interaction between the XD domain in P and the molecular recognition element (MoRE) (Fig. 1A) in N (4–7). The three-helix bundle in XD binds a helix from N′s MoRE element to facilitate this interaction (7). P has a second role: it binds N_{CORE} through its N-terminal soyuz1 motif (8) and performs a chaperone function required to keep newly synthesized N from binding to cellular RNA (9). This RNA-free N^0 is then transferred from the N^0-P complex to the nascent NC by a currently unknown mechanism.

Whereas the XD and MD domains of P have been well characterized, the interaction between the P N terminus and the N in the

Received 11 November 2015 **Accepted** 20 December 2015

Accepted manuscript posted online 30 December 2015

Citation Guryanov SG, Liljeroos L, Kasaragod P, Kajander T, Butcher SJ. 2016. Crystal structure of the measles virus nucleoprotein core in complex with an N-terminal region of phosphoprotein. J Virol 90:2849–2857. doi:10.1128/JVI.02865-15.

Editor: A. García-Sastre

Address correspondence to Sarah J. Butcher, sarah.butcher@helsinki.fi.

* Present address: Lassi Liljeroos, GlaxoSmithKline Vaccines, Siena, Italy.

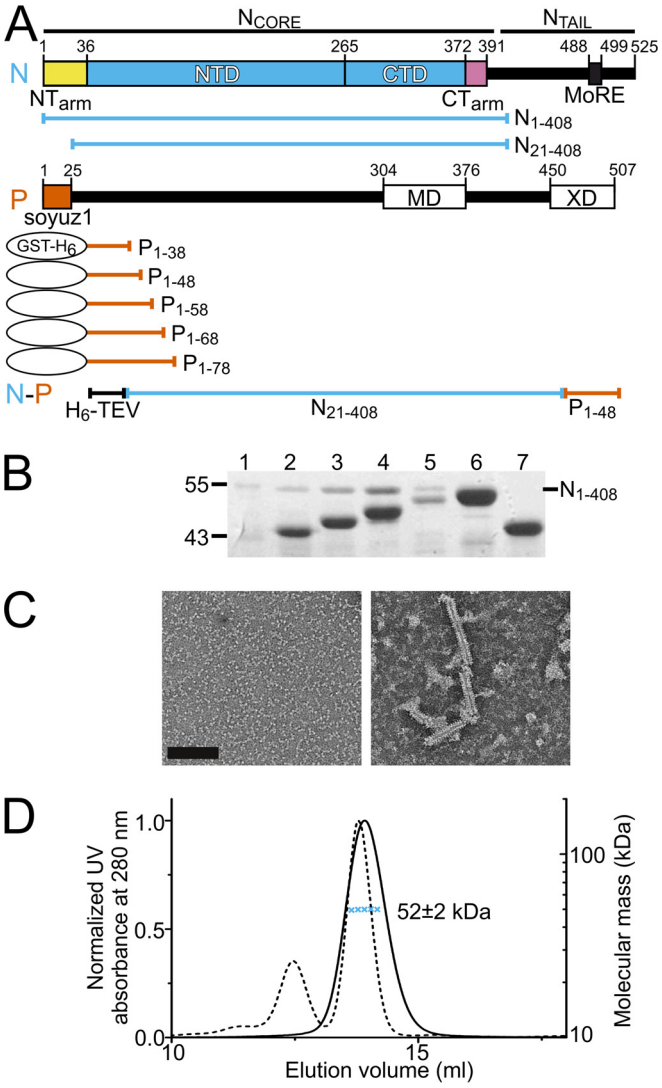

FIG 1 Protein constructs and N^0-P complex analysis. (A) Domain structure of measles N and P proteins and protein constructs used in this study. Numbers refer to amino acid positions. (B) Coexpressed N and GST-H_6-P constructs after elution from glutathione Sepharose beads. Lanes: 1, marker; 2, P_{1-38} and N_{1-408}; 3, P_{1-48} and N_{1-408}; 4, P_{1-58} and N_{1-408}; 5, P_{1-68} and N_{1-408}; 6, P_{1-78} and N_{1-408}; 7, GST-H_6 and N_{1-408}. Numbers on the left are molecular size markers. (C) Electron microscopy of negatively stained $N_{1-408}{}^0$–GST-H_6-P_{1-48} heterocomplex (left) and flowthrough from the glutathione Sepharose beads containing NC-like helical particles (right). Images are at the same scale. Scale bar, 100 nm. (D) Data from the SEC-MALLS experiment with the $N_{1-408}{}^0$–P_{1-48} heterocomplex after release from Ni-IMAC by enterokinase. The solid line is the absorbance profile; blue crosses show the molecular mass distribution. For comparison, the UV_{280} profile of the $N_{21-408}{}^0$–P_{1-48} chimera is shown with a dashed line.

N^0-P complex is less well described. The dual function for P has been established for many viruses of the *Mononegavirales* order, and the crystal structures of the vesicular stomatitis virus (VSV), Ebola virus, and Nipah virus (NiV) N^0-P complexes have been solved (10–12). In VSV N^0-P, the P N-terminal amino acids 17 to 31 formed an amphipathic α-helix and occupied a hinge region in N adjacent to the RNA-binding site (13). In NiV N^0-P, P amino acids 1 to 35 formed two α-helices separated by a kink (11). Interestingly, the NiV P binding site does not overlap the predicted RNA binding groove; therefore, the chaperoning mechanism of P appears to be remarkably different from that in VSV. In the present study, we addressed MeV N^0-P complex formation and structure. We expressed and purified MeV N^0-P complexes from *Escherichia coli* in a monodisperse form and mapped the location of the N-binding region on P to the first 48 N-terminal amino acids. Then we designed a chimeric N-P protein that was crystallized to reconstitute the N^0-P complex and solved the structure at a resolution of 2.7 Å. We also characterized the mode of interaction between the P N terminus and N^0 and showed the importance of hydrophobic interactions. Based on the structural data, we describe conformational changes upon RNA binding and propose a model for the preinitiation complex for RNA replication and transcription.

MATERIALS AND METHODS

Cloning and expression. All constructs were derived from reverse-transcribed N and P genes of an MeV wild-type isolate (a gift from I. Davidkin, Helsinki, Finland) (2). The N coding sequence was identical to the GenBank sequence for the Halonen strain (accession number U01996). The P coding sequence differed from GenBank sequence AF266288 for the Edmonston strain by three nucleotides: one was synonymous, and the other two resulted in the amino acids G225 and D492. Truncated P constructs were generated by PCR and cloned into NcoI and XhoI sites in pET41(a). The P constructs had an N-terminal glutathione *S*-transferase followed by a hexahistidine sequence (GST-H_6 tag) for purification. N_{1-408} and N_{21-408} were constructed similarly but were cloned into pET22(b) with a stop codon added to the 3′ end and did not contain any tags. For the N_{21-408}–P_{1-48} chimera, the N_{21-408} and P_{1-48} coding sequences were amplified by PCR to generate megaprimers with overlapping sequences. Then the megaprimers were annealed and extended. The product was amplified with primers coding for an N-terminal H_6-TEV tag, MGSSHHHHHHENLYFQ|S, where the tobacco etch virus (TEV) protease recognition sequence is underlined and the cleavage site is shown by a vertical line (14). A stop codon was introduced at the 3′ end. The product was cloned into NcoI and XhoI sites in pET22(b). Mutations in the P constructs were introduced by site-directed mutagenesis.

Proteins were expressed in *E. coli* Rosetta (DE3) (Merck Millipore). Expression was induced at an optical density at 600 nm (OD_{600}) of 0.5 with 0.5 mM isopropyl-β-D-thiogalactopyranoside (IPTG) and was allowed to proceed for 16 to 20 h at 22°C. Cells were collected by low-speed centrifugation and frozen at −80°C as pellets until use.

Protein purification. $N_{1-408}{}^0$ and GST-H_6-P_{1-48} were coexpressed in *E. coli* Rosetta (DE3). The cell pellet was resuspended in buffer A (20 mM Tris-HCl, 500 mM NaCl, 20 mM imidazole, 2 mM $CaCl_2$ [pH 8.0]) supplemented with 200 μg/ml of lysozyme and one EDTA-free protease inhibitor tablet/25 ml (Thermo Scientific). Cells were lysed with a French press at 22,000 lb/in^2, cell debris was spun down by low-speed centrifugation (11,000 × *g* for 15 min at 4°C), and the resulting supernatant was incubated with Ni-loaded IMAC beads (GE Healthcare) for 45 min at room temperature. After a washing with buffer A, the beads were exchanged into buffer B (20 mM Tris-HCl, 150 mM NaCl, 10 mM $MgCl_2$, 2 mM ATP [pH 8.0]) and incubated at 37°C for 10 min. Next, the beads were exchanged into buffer C (20 mM Tris-HCl, 150 mM NaCl, 2 mM $CaCl_2$ [pH 8.0]). The $N_{1-408}{}^0$–P_{1-48} heterocomplex was then released from the beads by an overnight digestion with enterokinase light chain (New England BioLabs). For 2 ml of Ni-IMAC beads with protein from 1 liter of cell culture, 0.16 μg of enzyme was used. The released protein was then concentrated with Millipore Amicon Ultra-4 30-kDa-cutoff spin concentrators and polished with size exclusion chromatography (SEC) using a Superdex 200 column (GE Healthcare). Peak fractions were collected and concentrated to the desired concentration with the same concentrator.

For $N_{21-408}{}^0$–P_{1-48} chimera purification, a cell pellet containing the

tagged chimera was resuspended in buffer D (20 mM Tris-HCl, 150 mM NaCl, 2 mM $MgCl_2$, 20 mM imidazole [pH 8.0]) supplemented with 10 μg/ml of lysozyme, 1 μg/ml of DNase I (Sigma-Aldrich), and 0.5 mM Pefabloc (Roche). Cells were lysed, and the lysate was cleared and incubated with Ni-IMAC as described above. After a washing with buffer D, protein was eluted with buffer D supplemented with 0.2 M imidazole. Eluted protein was incubated with TEV protease (purified in-house) overnight at 4°C. Cleaved protein was purified on a Superdex 200 column in buffer E (20 mM Tris-HCl, 150 mM NaCl [pH 8.0]), the monomer peak was collected, and uncleaved protein was removed by passing through an Ni-IMAC column. Purified protein was concentrated as described above.

N^0-P heterocomplex interaction experiments. To find the minimal length of P that stably interacted with N_{1-408}, 5 different P constructs were coexpressed with N_{1-408} as described above. The cells were lysed by sonication in phosphate-buffered saline (PBS) supplemented with 0.17 mg/ml of lysozyme. The cleared lysates were incubated with glutathione beads in PBS for 30 min at room temperature. After 3 washes with PBS, the proteins were eluted with 10 mM reduced glutathione in 50 mM Tris-HCl (pH 8.0).

To test the stability of the interactions, the purified $N_{1-408}{}^0$–GST-H_6–P_{1-48} heterocomplex was bound in 50 mM sodium phosphate (pH 7.4), 10 mM imidazole, and 300 mM NaCl to Ni-IMAC beads and eluted with 20 mM Tris (pH 8.0) supplemented with one of the following: NaCl at 0, 0.5, 1, or 2 M; KCl at 0.5, 1, or 2 M; urea at 2, 4, or 8 M; or Triton X-100 at 0.1% or 1%.

To probe $N_{21-408}{}^0$ heterocomplex formation with mutated GST-H_6-P constructs, cell lysates of individually expressed proteins were mixed and incubated overnight at 4°C. Lysate samples were incubated with Ni-IMAC beads and washed with lysis buffer E. The samples were eluted with buffer E supplemented with 0.2 M imidazole. Eluates were analyzed by SDS-PAGE.

SEC-MALLS experiment. To analyze the exact stoichiometry of the P_{1-48}–N_{1-408} heterodimeric complex, 47 μl of the complex (1 mg/ml) released by enterokinase digestion was run on a Superdex 200 10/300 GL column coupled into UV, refractive index, and multiangle laser light scattering (MALLS) detectors (Wyatt Technology). The molecular weight of the complex was then calculated based on the refractive index and MALLS signals using ASTRA 6 software (Wyatt Technology).

Electron microscopy of negatively stained samples. Samples were pipetted on glow-discharged carbon coated copper grids and stained with 1% (wt/vol) sodium phosphotungstate (pH 7.0). Grids were imaged with an FEI F20 transmission electron microscope, and images were collected with a Gatan Ultrascan 4000 charge-coupled-device (CCD) camera.

Structure determination. Crystals of the $N_{21-408}{}^0$–P_{1-48} chimeric protein were grown by sitting-drop vapor diffusion (22°C) by mixing 200 nl of protein (8 mg/ml) with 200 nl of reservoir (0.1 M sodium citrate [pH 5.2], 3% polyethylene glycol 8000). Crystals were cryoprotected in mother liquor containing 20% glycerol and flash-frozen in liquid nitrogen. Diffraction data were collected at the Diamond Light Source beamline I03. The data set was processed and scaled using the xia2 package (with XDS and AIMLESS) (15, 16). A summary of the data collection is given in Table 1. The structure was solved by molecular replacement using PHASER (17). The N-terminal domain (NTD) and C-terminal domain (CTD), corresponding to amino acids 31 to 261 and 262 to 71, respectively, of NiV N (PDB code 4CO6 [11]), were used as search models separately. The model was rebuilt using several cycles of autobuilding and refinement with PHENIX (18) and manual rebuilding with COOT (19). No density was observed for the N regions from 21 to 30, 119 to 120, and 133 to 139 and the P region from 39 to 48, and therefore, they were left out of the model. The last refinement cycles were done using TLS parameters (two TLS groups). The final refinement statistics are summarized in Table 1. The final R factors (R_{work}/R_{free}) of the refined structure are 21.1%/26.6% (Table 1). In the Ramachandran plot, 90% of the residues in the structure are in the most favored regions.

TABLE 1 Data collection and refinement statistics[a]

Parameter	Value(s)
Wavelength (Å)	0.9763
Resolution range (Å)	78.9–2.71 (2.807–2.71)[b]
Space group	P 3_1 2 1
Unit cell	a = 91.14, b = 91.14, c = 94.21, α = β = 90°, γ = 120°
Total reflections	63,741
Unique reflections	12,656
Multiplicity	5.1 (4.9)[b]
Completeness (%)	99.8 (99.5)[b]
Mean I/sigma(I)	7.5 (1.6)[b]
R_{merge}	11.2 (78.3)[b]
Reflections used for R_{free}	700
R_{work} (%)	21.1
R_{free} (%)	26.6
No. of nonhydrogen atoms	
Macromolecules	2,975
Water	9
Protein residues	407
RMSD	
Bond length (Å)	0.005
Bond angles (°)	0.976
Ramachandran favored (%)	90.52
Ramachandran outliers (%)	1.75
Average B-factor (Å^2)	
Protein	68.9
Solvent	49.6

[a] A synchrotron radiation source and Diamond Light Source beamline I03 were used.
[b] Statistics for the highest-resolution shell are shown in parentheses.

Structure analysis. All the structure illustrations were prepared using UCSF Chimera software (20). Interface surface was estimated using the PDBePISA server (21). Calculation of the relative angle between the N domains in N^0-P versus NC structure (PDB code 4UFT) was done using Modeller software (22) as described earlier (23). Structure alignments and root mean square deviation (RMSD) value calculations were made using UCSF Chimera. Dali multiple structural alignment (24) was used to generate the corresponding primary sequence alignment, followed by phylogenetic tree generation by PHYLIP in Unipro UGENE software (25).

Protein structure accession number. Final refined coordinates and structure factors have been deposited in the Protein Data Bank (PDB) under accession code 5E4V.

RESULTS

Mapping the interaction of the MeV $N_{CORE}{}^0$ with the N-terminal region of P and crystallization of the complex. In order to obtain a well-structured $N_{CORE}{}^0$-P complex, we analyzed the protease sensitivity of N by limited trypsin proteolysis (data not shown). Based on mass spectrometric analysis of the fragments observed, we cloned a C-terminally truncated construct containing the first 408 amino acids, N_{1-408}, thus excluding the disordered C-terminal N_{TAIL} region (7).

To screen for N_{CORE} interaction in the N-terminal region of P, we used coexpression of N_{1-408} together with GST-hexahistidine (GST-H_6) fusions with P_{1-38}, P_{1-48}, P_{1-58}, P_{1-68}, or P_{1-78} (Fig. 1A) and analyzed the interactions by GST affinity chromatography. All of the P constructs readily interacted with N_{1-408} and could be

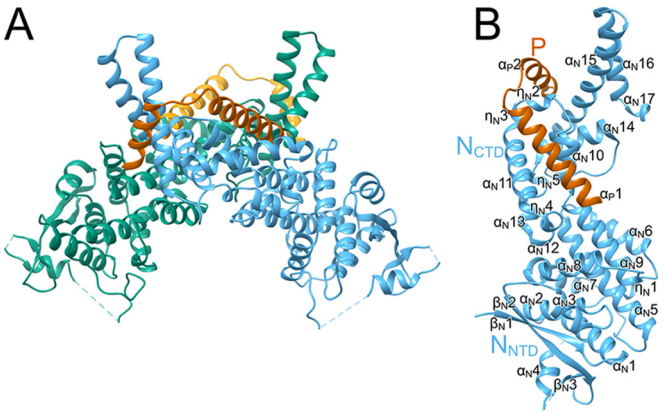

FIG 2 Crystal structure of MeV N^0-P complex. Shown is a cartoon representation of the chimeric $N_{21-408}{}^0$–P_{1-48} structure. (A) The crystallized dimer. Monomer 1 is sky blue and orange; monomer 2 is blue-green and orange-red. (B) The interaction of monomer 1 N (sky blue) and monomer 2 P (orange-red) fragments composing one N^0-P heterocomplex. Secondary structure elements are labeled.

clearly seen in SDS-PAGE (Fig. 1B). Thus, the P N-terminal interaction site with N_{CORE} resides within the first 38 amino acids. We analyzed negatively stained $N_{1-408}{}^0$–GST-H_6–P_{1-48} eluate and the flowthrough with electron microscopy. In the eluate we observed a monodisperse solution of a small complex (Fig. 1C, left), whereas in the flowthrough, NC-like helical particles were readily visible (Fig. 1C, right). Probably, the NC-like particles contained N assembled on nonspecific cellular RNA (26). After GST-H_6 tag cleavage, the purified complex was eluted from gel filtration as a single peak corresponding to a 1:1 heterodimer and was verified by SEC-MALLS to be 52 ± 2 kDa in size (Fig. 1D). This complex appeared not to contain nucleic acid, as the $A_{260/280}$ was 0.55, whereas the expected ratio for pure protein is ~0.6. Despite extensive efforts, the heterodimeric complex failed to crystallize. Hence, we designed a chimeric construct, H_6–TEV–$N_{21-408}{}^0$–P_{1-48}, in which the N-terminal region of P was directly fused to the C terminus of the N_{CORE} domain lacking its NT_{arm} region (Fig. 1A). The chimera was readily expressed as a soluble protein and purified. The gel filtration mobility (Fig. 1D) and the $A_{260/280}$ ratio of the chimera were similar to those of the heterodimeric complex, with an additional dimer peak. The solution state of the $N_{21-408}{}^0$–P_{1-48} chimera suggests that the P_{1-48} sequence is bound to the P-binding site reconstituting the N^0-P complex, preventing the formation of helical complexes.

Crystal structure of the MeV $N_{CORE}{}^0$-P complex. The MeV $N_{21-408}{}^0$–P_{1-48} chimera was crystallized in the space group $P3_121$ as a dimer with the P_{1-48} sequence swapped between chimera monomers. We determined the structure at a resolution of 2.7 Å by molecular replacement using the NiV N^0-P complex structure with PDB code 4CO6 (11) as a starting model (Fig. 2 and Table 1). The amino acid sequence of the $N_{21-408}{}^0$–P_{1-48} chimera could be traced starting from N residue 31 to P residue 38 with the exception of N residues 119 and 120 and 133 to 139. The buried surface interface in the crystallized dimer was 6,520 Å^2, indicating a stable interaction interface for the dimer as seen in gel filtration.

$N_{CORE}{}^0$ is primarily an α-helical protein with two domains, the NTD (amino acids 31 to 265) and the CTD (amino acids 266 to 372) (Fig. 2B) separated by a hinge. The NTD is formed by α-helices α_N1 to α_N9, one 3/10 helix η_N1, and parallel β-sheet β_N1-β_N2 with the adjacent short β-strand β_N3 (Fig. 2). The CTD is formed by helices α_N10 to α_N15 and four 3/10 helices, η_N2 to η_N5. The CT_{arm} (amino acids 373 to 408) continues as helices α_N15 to α_N17, with α_N15 and α_N16 adopting a helix-turn-helix conformation. P_{1-48} forms two helices (Fig. 2 and 3). The first helix, α_P1, is a continuation of the α_N17 helix and binds the partner molecule in the crystallized dimer to the groove formed by helices α_N10 and α_N11. The second helix, α_P2, contacts helix η_N2.

Interaction of $N_{CORE}{}^0$ with P is mainly hydrophobic. Conservation of the $N_{CORE}{}^0$ binding interface for P and of the P N-terminal region in some paramyxoviruses has been described previously (8, 11). In the MeV $N_{CORE}{}^0$-P complex, the binding interface is mostly composed of conserved hydrophobic residues (Fig. 3A and B, in blue). To biochemically probe the binding of the P N-terminal region to $N_{CORE}{}^0$, we screened for dissociation of N_{1-408} from GST-H_6–P_{1-48} bound on Ni-IMAC beads under different conditions and looked for release of N_{1-408}. The screen was designed to include conditions which would hinder either ionic or hydrophobic interactions between the proteins. NaCl or KCl concentrations ranging between 0 and 2 M did not cause significant release of N_{1-408}, whereas 0.1% and 1% Triton X-100 caused release of N_{1-408} from the complex (Fig. 3C) to levels similar to those obtained with 4 and 8 M urea, respectively.

To evaluate the role of P's hydrophobic amino acid residues in N^0 binding, we expressed N_{21-408} lacking the NT_{arm}. We found that N_{21-408} was insoluble and formed NC-like particles upon expression (data not shown), similar to N_{1-408}, but could bind to P_{1-48} *in vitro*. We pulled down N_{21-408} with GST-H_6-tagged wild-type P_{1-48} and its mutants (Fig. 3D). While wild-type P_{1-48} can efficiently bind N_{21-408}, replacements of hydrophobic by negatively charged amino acids (L13D, I16D, and L19E) severely affected the interaction. Replacement of L13 by the small amino acid Ala also strongly affected the interaction, possibly due to the increased solvent accessibility of the binding interface. In line with this observation, we still observed residual binding of the shorter P_{8-48} peptide where most of the interacting hydrophobic amino acids were retained (Fig. 3D, lane 9). Thus, hydrophobic interactions make a major contribution to P N-terminal region and $N_{CORE}{}^0$ binding.

Comparison of the MeV RNA-bound helical form with the chaperoned form. Direct comparison of the MeV $N_{CORE}{}^0$-P and helical NC structures reveals several factors that could contribute to P's chaperone activity; these include conformational changes (Fig. 4) as well as the position of P and RNA binding (Fig. 5 and 6). The largest difference between the two structures is that there is a relative domain movement in the MeV N in the $N_{CORE}{}^0$-P complex, compared to the helical RNA-bound NC form (Fig. 4A and B) (1). By aligning either the CTD or NTD only, we measured an ~40° relative rotation of the two domains, with the hinge occurring between α_N9 and α_N10 (Fig. 4). The RMSD for the individual domains in the two different MeV N conformations were calculated (Table 2). This comparison indicated that the 4.3-Å resolution cryo-EM structure agrees well with our crystal structure, and the changes seen between the structures could be interpreted reliably (Fig. 4A and B). Besides bending of the hinge between helices α_N9 and α_N10, helix α_N6 forming the lower lobe of the RNA binding cleft differs between the two different states. The helix undergoes both a shift and a rotation around its axis by half a turn (Fig. 4D). The helix movement increases the proximity of the two

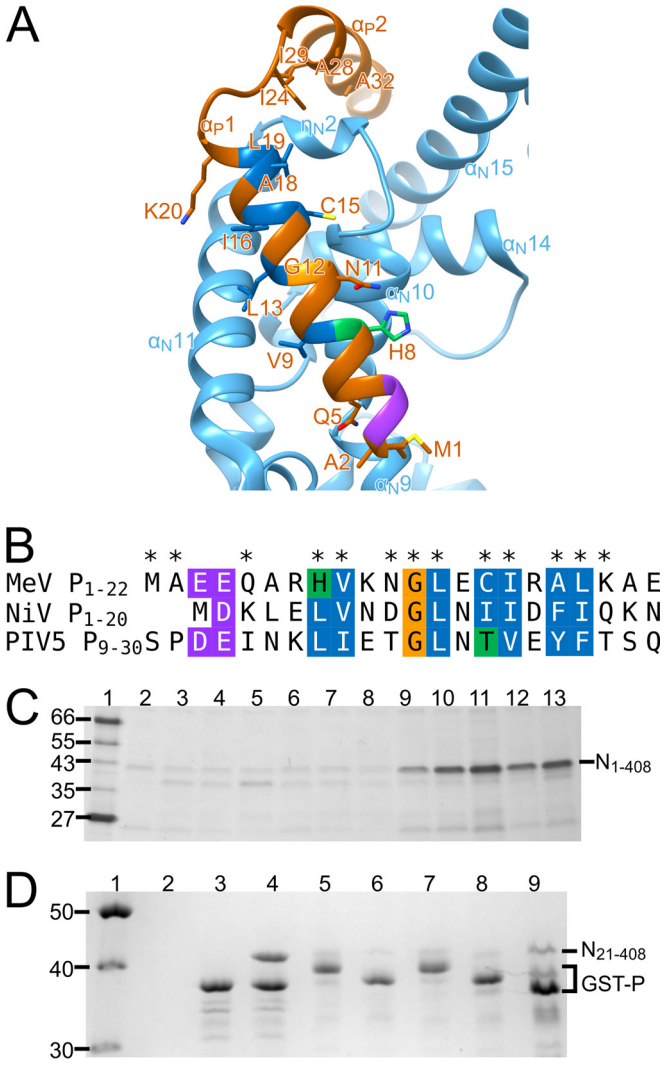

FIG 3 Hydrophobic interactions in N^0-P binding. (A) View of N_{21-408}–P_{1-48} binding interface in cartoon representation. The P (orange-red) residues interacting with N (sky blue) are shown in stick representation and labeled. Colors represent residues conserved throughout the *Paramyxovirinae* as follows: violet, acidic; green, polar; blue, hydrophobic; and orange, glycine (8). (B) Alignment of P N termini of MeV, NiV, and PIV5. Asterisks indicate residues making contacts with N^0. Conserved residues have a colored background. (C) SDS-PAGE of protein released from the N_{1-408}–GST-H_6–P_{1-48} heterodimer complex bound to Ni-IMAC beads when subjected to different conditions. Lanes: 1, marker; 2, 0 M NaCl; 3, 0.5 M NaCl; 4, 1 M NaCl; 5, 2 M NaCl; 6, 0.5 M KCl; 7, 1 M KCl; 8, 2 M KCl; 9, 2 M urea; 10, 4 M urea; 11, 8 M urea; 12, 0.1% Triton X-100; 13, 1% Triton X-100. (D) SDS-PAGE of pull-down of N_{21-408} by GST-H_6–P_{1-48} and its mutants. Lanes: 1, markers; 2, control N_{21-408} only; 3, control GST-H_6–P_{1-48wt} only; 4, N_{21-408} plus GST-H_6–P_{1-48wt}; 5, N_{21-408} plus GST-H_6–$P_{1-48\ L13D}$; 6, N_{21-408} plus GST-H_6–$P_{1-48\ L13A}$; 7, N_{21-408} plus GST-H_6–$P_{1-48\ I16D}$; 8, N_{21-408} plus GST-H_6–$P_{1-48\ L19E}$; 9, N_{21-408} plus GST-H_6–P_{8-48}. Note that some of the P mutations affected the electrophoretic mobility of the tagged constructs due to impaired SDS binding to the protein molecules with changed net charge (compare lanes 5 and 7 with lane 3). The deletion construct P_{8-48} migrates faster, reflecting its shorter amino acid sequence. Numbers on the left in panels C and D are molecular size markers.

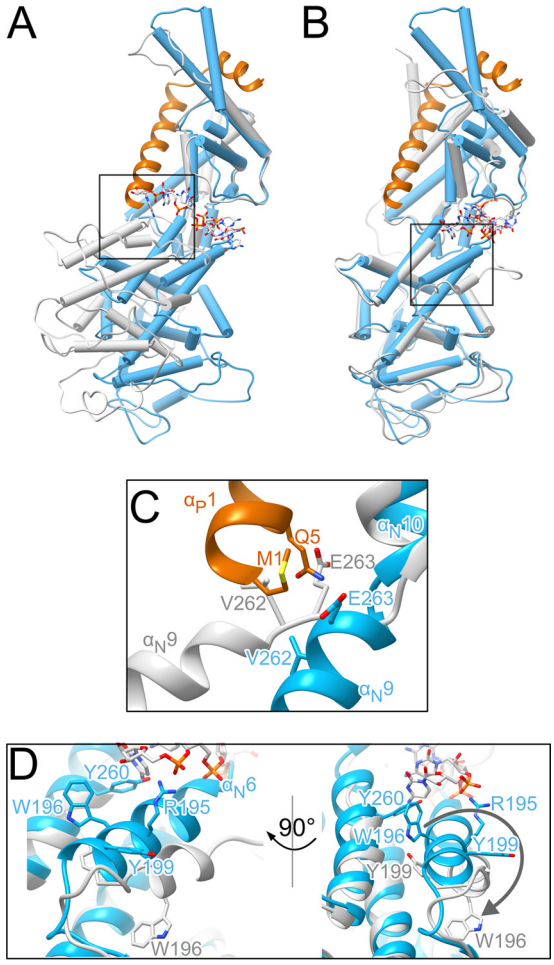

FIG 4 MeV N^0-P versus NC structure. Tube-and-plank representation of overlays of N^0-P (N, sky blue; P, orange-red) and NC model (light gray) with their CTDs (A) or NTDs (B) aligned. (C) Cartoon representation close-up view of hinge region boxed in panel A. (D) Cartoon representation close-up view of α_N6 helix boxed in panel B. The arrow on the right side shows hypothetical turn direction of α_N6 helix upon RNA binding.

sides of the interdomain cleft in $N_{CORE}{}^0$-P and therefore collapses the NC RNA-binding site. In addition, the surface electrostatic charge distribution changes quite dramatically depending on the α_N6 conformation. In $N_{CORE}{}^0$-P, a new negatively charged groove is evident on the NTD surface that could potentially bind RNA (Fig. 5). It has a contribution from the conserved R194 that interacts with the RNA backbone in NC (1). In NC, Y199 stacks with Y260, a key residue that regulates RNA binding pocket size. In $N_{CORE}{}^0$-P, Y199 faces the exterior and W196 occupies the space instead, thus potentially participating in the local stacking configuration.

Alignment of the N_{CTD} domains of $N_{CORE}{}^0$-P and NC (1) models (Fig. 4A and C) shows that the P N terminus would clash with helix α_N9 of N in the NC conformation; thus, the alternative conformation is favored. When we consider the superposition of N_{CTD}s in the context of the assembled NC, we can discern a direct effect of P binding (Fig. 6). The α_P1 helix overlaps the NT_{arm} of the N_{i-1} protomer and the α_P2 helix overlaps the CT_{arm} of the N_{i+1} protomer. Hence, P could specifically inhibit the association of adjacent protomers to the growing NC helix by steric hindrance, rather than by competing with the RNA-binding site.

Comparison to other virus nucleoproteins. Comparison of the N structures from MeV and other viruses of the *Mononegavirales* order reveals their structural similarity (Fig. 7). Each protein

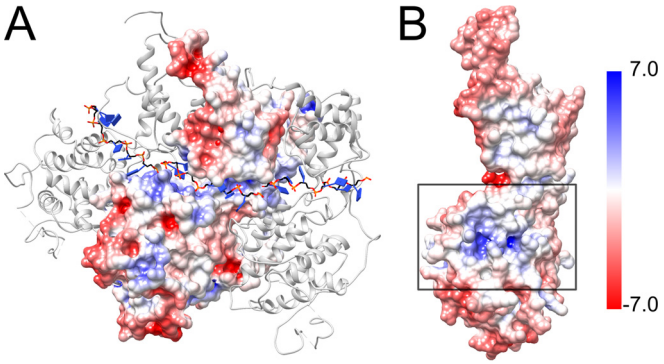

FIG 5 Potential alternative RNA-binding site. (A) Three consecutive N protomers of MeV NC, with the second protomer in a surface representation. The orientation is such that the outer surface of the nucleocapsid is facing the viewer. (B) N^0 surface representation in the same orientation as the second N protomer shown in panel A. Missing side chains in N^0 were added manually. Surface models are colored according to the electrostatic surface charge (positive, blue; negative, red). The positively charged patch in panel B is highlighted by a black box. The scale bar shows the electrostatic charge values.

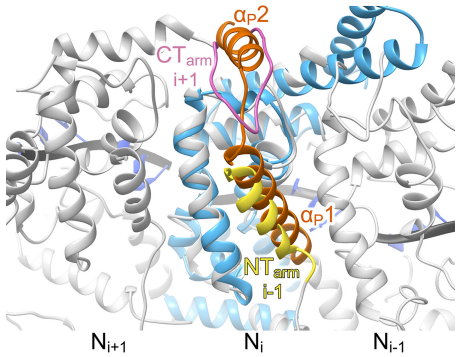

FIG 6 P interferes with NC assembly. The P_{1-48} fragment overlaps both the NT_{arm} and CT_{arm} of NC. Shown is a cartoon representation of superposed N^0-P (N^0, sky blue; P, orange-red) and NC (gray; PDB code 4UFT), NT_{arm} of the N_{i-1} protomer (yellow), and CT_{arm} of the N_{i+1} protomer (pink). Molecules were aligned using the N_{CTD} domains.

is composed of two domains with a single interdomain connection. Phylogenetic analysis based on Dali multiple structural alignment (24) shows that the two structurally closest to MeV N are NiV N and parainfluenza virus 5 (PIV5) N; MeV N shows 32% amino acid sequence identity to NiV N and 24% identity to PIV5 N.

To our knowledge, MeV and VSV are the only *Mononegavirales* members with both the N^0-P and N-RNA complexes available. Compared to the 40° rotation transition between the N^0-P and the RNA-bound states in MeV N, in VSV N, the RSMD reported between the two states was less than 1 Å (10), reflecting the fact that both VSV states were crystallized in a ring form that probably constrained the conformation. In contrast to MeV, VSV P blocks the RNA-binding site rather than binds on the opposite side of the molecule. For the other N^0-P complexes reported, NiV N^0-P is the closest, with a binding site similar to that for MeV N^0-P (Fig. 3 and 6), and relative domain positioning (referred to as an "open conformation" in NiV [11]). None of the other RNA-bound states are from a helical NC structure; rather, they are all ring structures, but in PIV5, RSV, and rabies virus, the RNA-bound states also indicate domain positioning similar to that of MeV NC ("closed state") (11, 27). These comparisons emphasize the importance of the flexibility in the interdomain region in regulating N′s interactions with other viral components.

DISCUSSION

Here, for the first time in paramyxovirus research, our data allow direct comparison of the structures of the nucleoprotein from the same virus in two functional states: a P-bound naive state and an RNA-bound helical assembly. Our X-ray crystallographic atomic model at higher resolution confirms, complements, and improves upon the recently published cryo-EM reconstruction (1). The overall fold of MeV N is most similar to those of NiV and PIV5 N proteins (Fig. 7) (11, 27). In addition, the structure of MeV P_{1-48} and its binding site are very similar to those of NiV N^0-P complex (11). Noting the extensive, conserved hydrophobic interactions of the P protein helix α_P1 and N (8, 11), we showed by mutation of the hydrophobic residues in P and by biochemical analyses that we could indeed impair the binding interaction.

Our findings suggest that both N domains mostly preserve their fold upon transition from the N^0-P to the NC state. Notably, N in both N^0-P and NC has a flexible region between residues 118 and 140 composed of a well-defined α_N4 helix (residues 124 to 130) flanked by unresolved regions. In NiV N, the α_N4 helix is longer and only one unresolved region was left, whereas in PIV5, there are no gaps here. This region is on the outer surface of the NC. Hence, this flexible region could interact with the flexible C terminus of N or with the polymerase complex.

How does P act as a chaperone? The roles of P are at least 2-fold: first, to act as a chaperone to keep N^0 in its RNA-free, soluble, monomeric form, and second, to position the polymerase complex for polymerization. In the role as a chaperone, it has been proposed that in the NiV N^0-P complex, binding of P to N locks the open conformation by rigidifying the N_{CTD} structure (11). Our model, however, suggests a significant impact from steric interference between the P N terminus and N_{NTD} (Fig. 6). Alignment of the N_{CTD} domains of the MeV N^0-P and NC (1) models (Fig. 4A and C) shows that the P N terminus will clash with helix α_N9 of N in the RNA-bound conformation, thus favoring the RNA-free conformation in N^0-P. The flexibility of the N molecule is therefore an inherently important part of our model, compared to the published NiV model (11). We have additional evidence that in the NC, N can assume different conformations. The pitch of the protease-treated NC used for high-resolution structure determination is 5.0 nm (1) and imposes a rigidity on the helix that was important for image processing. However, the recombinant full-length protein forms flexible helices with pitches ranging from 5.0 to 6.6 nm (28, 29), and those imaged inside virions have a pitch of 6.4 nm (2). In the latter, the rigidity of the NC helix is enforced by interaction with an outer layer of matrix protein. Where the matrix is lacking, the NC is flexible. From the current work, at least two flexible regions could affect the twist and pitch, the twisting of the two domains (28), induced by the interdomain hinge region described above, and the conformation of the α_N6 helix. Confident assignment of amino acids Trp196 and Tyr199 in this helix in both the cryo-EM and X-ray electron densities showed rotation and elongation of the α_N6 helix (Fig. 4D), reflecting the intrinsic flexibility in this part of the molecule. Noticeably, in both the NiV N^0-P and PIV5 N-RNA structures (11, 27), a loop preceding the corresponding helix is unresolved; this loop flexibility further supports the inherent mobility of the α_N6 helix.

TABLE 2 RMSD values between N structures of MeV N^0-P and MeV NC, NiV N^0-P, or PIV5 N-RNA complexes[a]

MeV N^0 domain	RMSD MeV N^0-P vs MeV NC	RMSD MeV N^0-P vs NiV N^0-P	RMSD MeV N^0-P vs PIV5 N-RNA
NTD (aa 31–265)	164 Cα pairs: 1.2 Å 220 Cα pairs: 2.7 Å	149 Cα pairs: 1.0 Å 215 Cα pairs: 2.6 Å	130 Cα pairs: 1.2 Å 221 Cα pairs: 3.2 Å
CTD (aa 266–372)	85 Cα pairs: 1.1 Å 107 Cα pairs: 1.9 Å	83 Cα pairs: 0.8 Å 107 Cα pairs: 1.7 Å	91 Cα pairs: 0.9 Å 107 Cα pairs: 1.8 Å

[a] The first item in each cell shows the number of Cα pairs used for alignment in UCSF Chimera and the corresponding RMSD value; the second item shows the number of all possible Cα pairs and the corresponding RMSD value. PDB codes and resolutions: MeV NC, 4UFT and 4.3 Å; NiV N^0-P, 4CO6 and 2.5 Å; and PIV5 N-RNA, 4XJN and 3.11 Å.

What determines whether N binds P or RNA? The RNA binding in the NC state is favored by specific arrangement of the amino acid residues from both the N_{NTD} and N_{CTD} (1). In the N^0-P state, the rotation of the N domains forces the overlap of these two binding surfaces; hence, we hypothesize that the RNA binding affinity is reduced. This is supported by two observations. First, regarding the solubility of the chimera in an *E. coli* cell lysate, we found a predominance of RNA-free monomers and dimers rather than helical assemblies, even in the presence of *E. coli* RNA, compared to what was found with N expressed alone. Hence, the N^0-P interaction hampered NC assembly and binding to RNA in our study. Second, the surface charge distribution of the chimera is altered, changing and shrinking the position of the positively charged surface in the N^0-P compared to the NC. This suggests that N′s affinity for P in our constructs was higher than for RNA. There is probably a balance in the cell, during infection, dictated by the local concentrations of the relevant components and the avidity of N for RNA and its neighboring N subunits that together orchestrate the assembly of the NC. The flexibility of N facilitates its exchange between its binding partners, P and RNA. P can further regulate helix assembly through sterically impeding both side-to-side and vertical growth of the helix through occupying the same sites as both the NT_{arm} of the N_{i-1} protomer and CT_{arm} of the N_{i+1} protomer (Fig. 6).

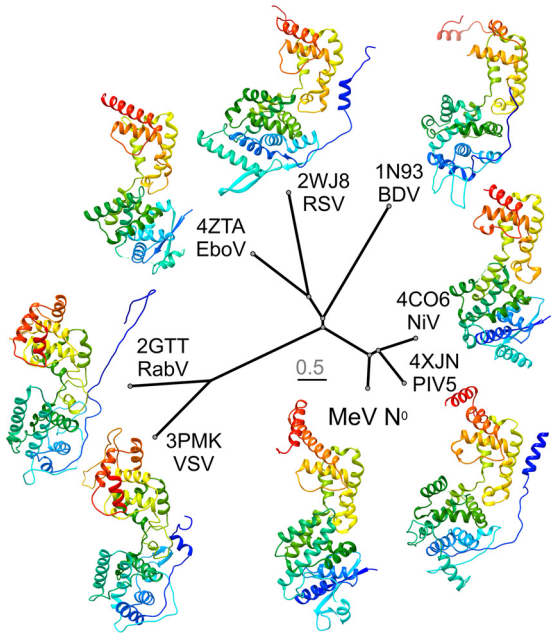

FIG 7 Phylogenetic analysis of N structures. Shown is a phylogenetic comparison of the MeV N^0 structure with the other published *Mononegavirales* nucleoprotein structures as a nonrooted tree. The scale bar corresponds to the number of expected substitutions per amino acid site between nodes. Atomic models are aligned by their CTDs and shown in ribbon representation. PDB codes are given above the virus abbreviations.

Model for the formation of a preinitiation complex. According to the current paramyxovirus models, both transcription and replication are initiated at the 3′ end of the genomic RNA (30). The linear unidirectional organization of the "herringbone" NC means that the 3′ and 5′ ends of the NC do not present the same molecular surface due to this polarity. In addition, the transition between the bulk of the helix to the tip means that there is an extra potential site for P binding on the last molecule of the NC at the 3′ end (Fig. 8). The specific architecture of the pointed 3′ end of the NC could thus facilitate the recognition of the initiation site and assembly of the preinitiation complex through the interactions of P, L, N, and RNA. We propose a simple model for formation of a preinitiation complex, as shown in Fig. 8. In this model, the first interactions occur between the RNA polymerase complex, L-P, and NC through P's XD domains (Fig. 1A) in a low-affinity interaction with the flexible extended N_{TAIL}s (5, 31). This transient interaction allows one-dimensional diffusion of the polymerase complex along the NC. The accurate positioning on the tip occurs when the P N-terminal region binds to a vacant NT_{arm} binding site at the NC's 3′ end. Binding of P may initiate NC uncoiling, as has been observed with mumps virus (32), to facilitate the release of the genomic RNA 3′ end from the RNA-binding groove. RNA release from the NC 3′ end by P is indirectly supported by the ability of the P N-terminal region to dissociate the N_{21-408} assembly where effectively all NT_{arm} sites are vacant (Fig. 3D). Upon RNA 3′-end release, it may transiently bind to the exposed positively charged patch on N by its sugar-phosphate backbone (Fig. 5). The polymerase complex is then positioned for the entry of the first 6 nucleotides of the RNA 3′ end in to the active site of L (33–35). Bipartite promoter recognition by the polymerase complex is required for genomic RNA replication (36). In analogy to mumps virus, this may require further uncoiling of the NC, promoted by P (32). Elongation will also require NC uncoiling to expose the RNA. The processivity of the polymerase complex will promote this, and additional P may be injected into the helical assembly, resulting in local NC uncoiling and template RNA exposure according to the cartwheel model (37). N could be recycled onto the NC once the polymerase complex has passed due to the transient association with the P CTD. The presence of assembled matrix on the NC during early stages of infection will necessitate additional disassembly which is as yet not understood.

In conclusion, our MeV N^0-P structure and its comparison to

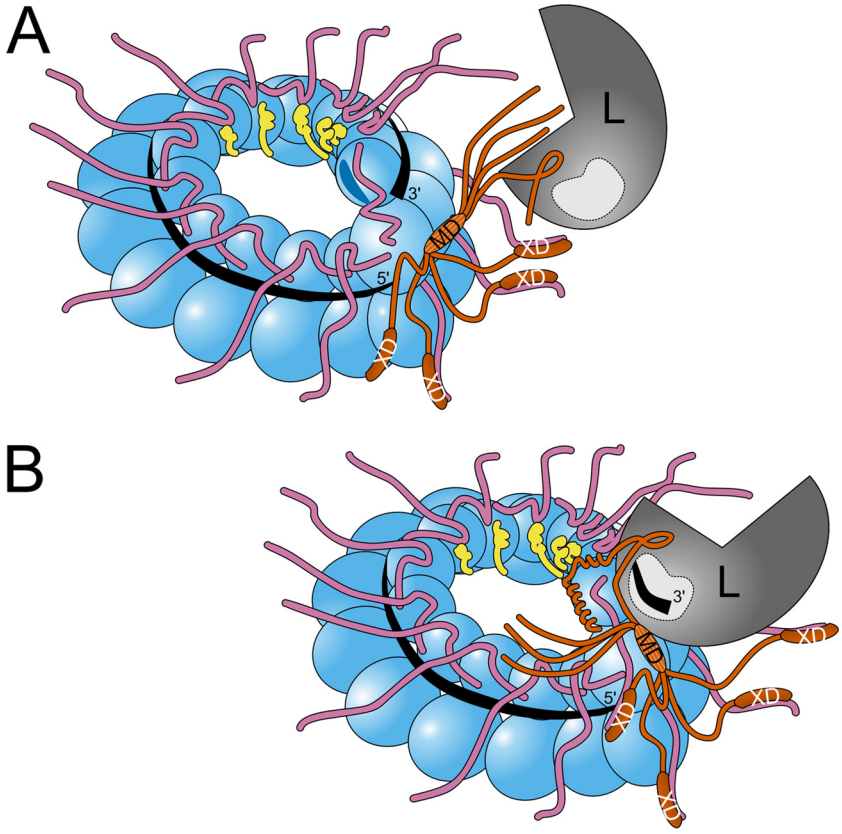

FIG 8 Schematic model of RNA synthesis preinitiation complex formation. (A) Model of nonspecific binding of the polymerase complex to NC. The NC is composed of genomic RNA (black ribbon) and the N protomers, in which the N_{CORE} domains are depicted as sky blue peanut shapes, NT_{arm} in yellow, and N_{TAIL} in pink. A complex of polymerase subunit L (gray) with the P tetramer (orange-red) binds the NC through the interaction of P's XD domains with MoRE motifs in N_{TAIL}s. There is a vacant P/NT_{arm} site on the 3′ protomer of the NC (dark blue crescent). (B) Model of the preinitiation complex formation. One of the P N termini occupies the P/NT_{arm} site on the 3′ protomer of the NC. Binding results in release of the RNA 3′ end, which is then positioned in the polymerase catalytic site to form a preinitiation complex.

the previously reported NC state provide insight into MeV NC assembly and polymerase activity.

ACKNOWLEDGMENTS

We thank the following people for their help: Eevakaisa Vesanen for electron microscopy, Juho Kellosalo for SEC-MALLS experiments, Tuula Nyman for mass spectrometry, and the Finnish Instruct National Associate Center, the National Biocenter Finland Cryo-Electron Microscopy Unit, the Crystallization Facility, and the Proteomics and Metabolomics Unit for the use of their facilities.

FUNDING INFORMATION

Sigrid Juselius Foundation provided funding to Sarah Jane Butcher. Biocenter Finland provided funding to Tommi Kajander and Sarah Jane Butcher. Suomen Akatemia (Academy of Finland) provided funding to Sarah Jane Butcher under grant numbers 139178 and 275199.

L.L. was a fellow of the Viikki Doctoral Programme in Molecular Biosciences. The Diamond Light Source beam line I03 is acknowledged for provision of synchrotron beam time. The research leading to these results received funding from the European Community's Seventh Framework Programme (FP7/2007-2013) under BioStruct-X (grant agreement no. 283570). The funders had no role in study design, data collection and interpretation, or the decision to submit the work for publication.

REFERENCES

1. **Gutsche I, Desfosses A, Effantin G, Ling WL, Haupt M, Ruigrok RW, Sachse C, Schoehn G.** 2015. Near-atomic cryo-EM structure of the helical measles virus nucleocapsid. Science **348:**704–707. http://dx.doi.org/10.1126/science.aaa5137.
2. **Liljeroos L, Huiskonen JT, Ora A, Susi P, Butcher SJ.** 2011. Electron cryotomography of measles virus reveals how matrix protein coats the ribonucleocapsid within intact virions. Proc Natl Acad Sci U S A **108:**18085–18090. http://dx.doi.org/10.1073/pnas.1105770108.
3. **Communie G, Crépin T, Maurin D, Jensen MR, Blackledge M, Ruigrok RW.** 2013. Structure of the tetramerization domain of measles virus phosphoprotein. J Virol **87:**7166–7169. http://dx.doi.org/10.1128/JVI.00487-13.
4. **Gely S, Lowry DF, Bernard C, Jensen MR, Blackledge M, Costanzo S, Bourhis J-M, Darbon H, Daughdrill G, Longhi S.** 2010. Solution structure of the C-terminal X domain of the measles virus phosphoprotein and interaction with the intrinsically disordered C-terminal domain of the nucleoprotein. J Mol Recognit **23:**435–447. http://dx.doi.org/10.1002/jmr.1010.
5. **Jensen MR, Communie G, Ribeiro EA, Jr, Martinez N, Desfosses A, Salmon L, Mollica L, Gabel F, Jamin M, Longhi S, Ruigrok RW, Blackledge M.** 2011. Intrinsic disorder in measles virus nucleocapsids. Proc Natl Acad Sci U S A **108:**9839–9844. http://dx.doi.org/10.1073/pnas.1103270108.
6. **Johansson K, Bourhis J-M, Campanacci V, Cambillau C, Canard B, Longhi S.** 2003. Crystal structure of the measles virus phosphoprotein domain responsible for the induced folding of the C-terminal domain of the nucleoprotein. J Biol Chem **278:**44567–44573. http://dx.doi.org/10.1074/jbc.M308745200.
7. **Kingston RL, Hamel DJ, Gay LS, Dahlquist FW, Matthews BW.** 2004. Structural basis for the attachment of a paramyxoviral polymerase to its template. Proc Natl Acad Sci U S A **101:**8301–8306. http://dx.doi.org/10.1073/pnas.0402690101.

8. **Karlin D, Belshaw R.** 2012. Detecting remote sequence homology in disordered proteins: discovery of conserved motifs in the N-termini of Mononegavirales phosphoproteins. PLoS One **7:**e31719. http://dx.doi.org/10.1371/journal.pone.0031719.
9. **Harty RN, Palese P.** 1995. Measles virus phosphoprotein (P) requires the NH_2- and COOH-terminal domains for interactions with the nucleoprotein (N) but only the COOH terminus for interactions with itself. J Gen Virol **76:**2863–2867. http://dx.doi.org/10.1099/0022-1317-76-11-2863.
10. **Leyrat C, Yabukarski F, Tarbouriech N, Ribeiro EA, Jr, Jensen MR, Blackledge M, Ruigrok RW, Jamin M.** 2011. Structure of the vesicular stomatitis virus N^0-P complex. PLoS Pathog **7:**e1002248. http://dx.doi.org/10.1371/journal.ppat.1002248.
11. **Yabukarski F, Lawrence P, Tarbouriech N, Bourhis JM, Delaforge E, Jensen MR, Ruigrok RW, Blackledge M, Volchkov V, Jamin M.** 2014. Structure of Nipah virus unassembled nucleoprotein in complex with its viral chaperone. Nat Struct Mol Biol **21:**754–759. http://dx.doi.org/10.1038/nsmb.2868.
12. **Kirchdoerfer RN, Abelson DM, Li S, Wood MR, Saphire EO.** 2015. Assembly of the Ebola virus nucleoprotein from a chaperoned VP35 complex. Cell Rep **12:**140–149. http://dx.doi.org/10.1016/j.celrep.2015.06.003.
13. **Green TJ, Zhang X, Wertz GW, Luo M.** 2006. Structure of the vesicular stomatitis virus nucleoprotein-RNA complex. Science **313:**357–360. http://dx.doi.org/10.1126/science.1126953.
14. **Carrington JC, Dougherty WG.** 1988. A viral cleavage site cassette: identification of amino acid sequences required for tobacco etch virus polyprotein processing. Proc Natl Acad Sci U S A **85:**3391–3395. http://dx.doi.org/10.1073/pnas.85.10.3391.
15. **Kabsch W.** 2010. XDS. Acta Crystallogr D Biol Crystallogr **66:**125–132. http://dx.doi.org/10.1107/S0907444909047337.
16. **Evans PR, Murshudov GN.** 2013. How good are my data and what is the resolution? Acta Crystallogr D Biol Crystallogr **69:**1204–1214. http://dx.doi.org/10.1107/S0907444913000061.
17. **McCoy AJ, Grosse-Kunstleve RW, Adams PD, Winn MD, Storoni LC, Read RJ.** 2007. Phaser crystallographic software. J Appl Crystallogr **40:**658–674. http://dx.doi.org/10.1107/S0021889807021206.
18. **Adams PD, Afonine PV, Bunkóczi G, Chen VB, Davis IW, Echols N, Headd JJ, Hung LW, Kapral GJ, Grosse-Kunstleve RW, McCoy AJ, Moriarty NW, Oeffner R, Read RJ, Richardson DC, Richardson JS, Terwilliger TC, Zwart PH.** 2010. PHENIX: a comprehensive Python-based system for macromolecular structure solution. Acta Crystallogr D Biol Crystallogr **66:**213–221. http://dx.doi.org/10.1107/S0907444909052925.
19. **Emsley P, Lohkamp B, Scott WG, Cowtan K.** 2010. Features and development of Coot. Acta Crystallogr D Biol Crystallogr **66:**486–501. http://dx.doi.org/10.1107/S0907444910007493.
20. **Pettersen EF, Goddard TD, Huang CC, Couch GS, Greenblatt DM, Meng EC, Ferrin TE.** 2004. UCSF Chimera—a visualization system for exploratory research and analysis. J Comput Chem **25:**1605–1612. http://dx.doi.org/10.1002/jcc.20084.
21. **Krissinel E, Henrick K.** 2007. Inference of macromolecular assemblies from crystalline state. J Mol Biol **372:**774–797. http://dx.doi.org/10.1016/j.jmb.2007.05.022.
22. **Sali A, Blundell TL.** 1993. Comparative protein modelling by satisfaction of spatial restraints. J Mol Biol **234:**779–815. http://dx.doi.org/10.1006/jmbi.1993.1626.
23. **Pandurangan AP, Shakeel S, Butcher SJ, Topf M.** 2014. Combined approaches to flexible fitting and assessment in virus capsids undergoing conformational change. J Struct Biol **185:**427–439. http://dx.doi.org/10.1016/j.jsb.2013.12.003.
24. **Holm L, Rosenstrom P.** 2010. Dali server: conservation mapping in 3D. Nucleic Acids Res **38:**W545–W549. http://dx.doi.org/10.1093/nar/gkq366.
25. **Okonechnikov K, Golosova O, Fursov M, and the UGENE team.** 2012. Unipro UGENE: a unified bioinformatics toolkit. Bioinformatics **28:**1166–1167. http://dx.doi.org/10.1093/bioinformatics/bts091.
26. **Spehner D, Drillien R, Howley PM.** 1997. The assembly of the measles virus nucleoprotein into nucleocapsid-like particles is modulated by the phosphoprotein. Virology **232:**260–268. http://dx.doi.org/10.1006/viro.1997.8568.
27. **Alayyoubi M, Leser GP, Kors CA, Lamb RA.** 2015. Structure of the paramyxovirus parainfluenza virus 5 nucleoprotein-RNA complex. Proc Natl Acad Sci U S A **112:**E1792–E1799. http://dx.doi.org/10.1073/pnas.1503941112.
28. **Bhella D, Ralph A, Yeo RP.** 2004. Conformational flexibility in recombinant measles virus nucleocapsids visualised by cryo-negative stain electron microscopy and real-space helical reconstruction. J Mol Biol **340:**319–331. http://dx.doi.org/10.1016/j.jmb.2004.05.015.
29. **Desfosses A, Goret G, Farias Estrozi L, Ruigrok RW, Gutsche I.** 2011. Nucleoprotein-RNA orientation in the measles virus nucleocapsid by three-dimensional electron microscopy. J Virol **85:**1391–1395. http://dx.doi.org/10.1128/JVI.01459-10.
30. **Noton SL, Fearns R.** 2015. Initiation and regulation of paramyxovirus transcription and replication. Virology **479-480:**545–554.
31. **Shu Y, Habchi J, Costanzo S, Padilla A, Brunel J, Gerlier D, Oglesbee M, Longhi S.** 2012. Plasticity in structural and functional interactions between the phosphoprotein and nucleoprotein of measles virus. J Biol Chem **287:**11951–11967. http://dx.doi.org/10.1074/jbc.M111.333088.
32. **Cox R, Pickar A, Qiu S, Tsao J, Rodenburg C, Dokland T, Elson A, He B, Luo M.** 2014. Structural studies on the authentic mumps virus nucleocapsid showing uncoiling by the phosphoprotein. Proc Natl Acad Sci U S A **111:**15208–15213. http://dx.doi.org/10.1073/pnas.1413268111.
33. **Liang B, Li Z, Jenni S, Rahmeh AA, Morin BM, Grant T, Grigorieff N, Harrison SC, Whelan SP.** 2015. Structure of the L protein of vesicular stomatitis virus from electron cryomicroscopy. Cell **162:**314–327. http://dx.doi.org/10.1016/j.cell.2015.06.018.
34. **Butcher SJ, Grimes JM, Makeyev EV, Bamford DH, Stuart DI.** 2001. A mechanism for initiating RNA-dependent RNA polymerization. Nature **410:**235–240. http://dx.doi.org/10.1038/35065653.
35. **Salgado PS, Makeyev EV, Butcher SJ, Bamford DH, Stuart DI, Grimes JM.** 2004. The structural basis for RNA specificity and Ca2+ inhibition of an RNA-dependent RNA polymerase. Structure **12:**307–316. http://dx.doi.org/10.1016/j.str.2004.01.012.
36. **Tapparel C, Maurice D, Roux L.** 1998. The activity of Sendai virus genomic and antigenomic promoters requires a second element past the leader template regions: a motif (GNNNNN)3 is essential for replication. J Virol **72:**3117–3128.
37. **Curran J.** 1998. A role for the Sendai virus P protein trimer in RNA synthesis. J Virol **72:**4274–4280.